Dual-Band MIMO Antenna with Enhanced Isolation for Sub-6 GHz 5G and Wi-Fi Applications

Yem Vu-Van, Thao Hoang-Thi-Phuong, Quyen Nguyen-Xuan, and Cuong Do-Manh

***Abstract*—This paper presents a single-layer dual-band multiple-input-multiple-output (MIMO) antenna with high isolation characteristics for the Sub-6 GHz n79 5G NR band (4.4–5.0 GHz) and 5-GHz Wi-Fi applications. The dual-band MIMO element consists of four-square patches with embedded slots, which are capacitively excited by a probe-fed patch at the center. To achieve high isolation, shorting vias are employed to produce a transmission zero for mutual coupling reduction at both operating frequency bands. The proposed two-port antenna achieves an overall size of $0.94\lambda \times 0.47\lambda \times 0.02\lambda$ at the lowest band of 4.6 GHz. Experimental results show measured bandwidths of 2.8% (4.62 - 4.75 GHz) and 3.9% (5.50 - 5.72 GHz) for the lower and upper bands, respectively. The antenna consistently provides more than 25 dB isolation, together with gains of 4.8–5.4 dBi for the 4.6 GHz band and 5.2–6.8 dBi for the 5.6 GHz band at both individual ports. The proposed design effectively covers the 4.62–4.75 GHz portion of the n79 band and the 5.50–5.72 GHz range for 5-GHz Wi-Fi, accommodating channel bandwidths up to 100 and 160 MHz, respectively.**

Link to graphical and video abstracts, and to code:
https://latamt.ieeer9.org/index.php/transactions/article/view/11038

***Index Terms*—Dual-band, high isolation, MIMO, WiFi, compact, single layer.**

I. Introduction

THE increasing demand for high-speed and reliable wireless communication has motivated the development of dual-band antennas for Sub-6 GHz 5G and WiFi applications [1], [2]. Since modern wireless devices must support multiple standards within limited space, dual-band operation can reduce hardware complexity while maintaining stable radiation performance. In addition, multiple-input multiple-output (MIMO) technology is essential for improving channel capacity, data rate, link reliability, and resistance to multipath fading. Therefore, a dual-band MIMO antenna is highly desirable for next-generation wireless terminals, access points, and IoT devices.

One of the most challenging tasks in designing a dual-band MIMO antenna is achieving high isolation 5-GHz Wi-Fi. Various decoupling networks have been reported in [3]–[8], including neutralization techniques [3], [4], multiple stubs [5], [6], and coupling elements [7], [8]. Although these methods can effectively suppress mutual coupling between MIMO elements, they are mainly suitable for monopole- or PIFA-based antennas. Such antennas generally exhibit omni-directional radiation patterns with relatively low gain, which limits their suitability for point-to-point links and long-range communication applications.

To address these limitations, several microstrip patch-based dual-band MIMO antennas have been developed for 5G and WLAN applications [9]–[16]. These designs can provide high-gain broadside radiation using multiple patch modes, slots, stubs, parasitic elements, DGS, SRR, or metasurface-based structures. However, achieving high isolation at both bands often requires multilayer structures, high profiles, or complex decoupling configurations. Therefore, a simple, single-layer, low-profile dual-band MIMO antenna with high isolation is still highly desirable.

To address the aforementioned limitations, several single-layer dual-band MIMO antennas have been reported in [17]–[21]. In these designs, dual-band operation is commonly realized by etching various slots on the main patch, such as U-shaped slots [17], [18], embedding complementary split-ring resonators [19], or employing multi-resonant radiators [20], [21]. Meanwhile, high isolation is achieved by inserting decoupling networks between the MIMO elements [17], [18] or arranging the elements in an orthogonal configuration [19]–[21]. Despite their potential for dual-band MIMO applications, these antennas still suffer from several drawbacks, including limited isolation, large element spacing, or unstable radiation patterns at the two operating bands.

In this paper, a single-layer dual-band MIMO antenna with high isolation is proposed. The MIMO element consists of four-square patches with embedded slots, which are capacitively excited by a centrally located probe-fed patch. To suppress mutual coupling 5-GHz Wi-Fi, shorting vias are introduced as compact decoupling structures, enabling high isolation without requiring additional space for decoupling networks. This distinguishes the proposed decoupling design from those in [17]–[21], which require more complex feeding structures while providing only limited isolation improvement. The proposed two-port antenna has a compact overall size of $0.94\lambda \times 0.47\lambda \times 0.02\lambda$. It operates effectively at 4.6 and 5.6 GHz, with isolation better than 25 dB and gain higher than 4.8 and 5.2 dBi across both bands.

The associate editor coordinating the review of this manuscript and approving it for publication was Roberto S. Murphy (*Corresponding author: Thi Phuong Thao Hoang).*

Y. Vu-Van, and Q. Nguyen-Xuan are with the School of Electrical and Electronic Engineering, Hanoi University of Science and Technology, Hanoi, Vietnam (e-mails: yem.vuvan@hust.edu.vn, and quyen.nguyenxuan@hust.edu.vn).

Thao Hoang-Thi-Phuong is with the Faculty of Electronics and Telecommunications, Electric Power University, Hanoi, Vietnam (e-mail: thaohp@epu.edu.vn).

C. Do-Manh is with the Faculty of Electrical and Electronic Engineering, Phenikaa School of Engineering, Phenikaa University, Hanoi 12116, Vietnam (e-mail: cuong.domanh@Phenikaa-uni.edu.vn).

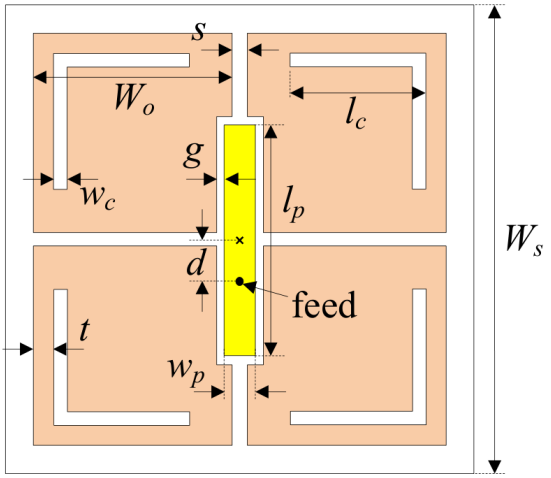


Fig. 1. Geometry of the dual-band antenna.

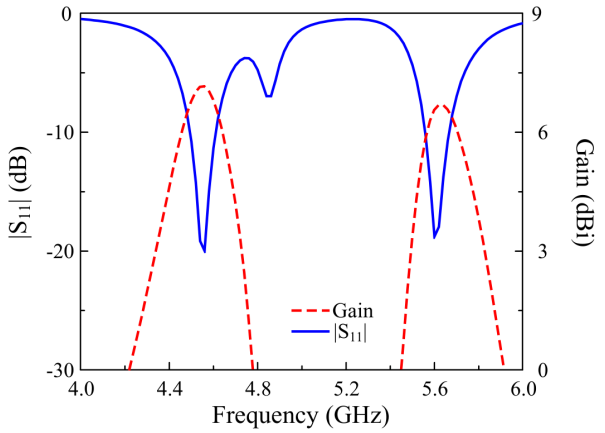


Fig. 2. Simulated $|S_{11}|$ and realized gain of the dual-band antenna.

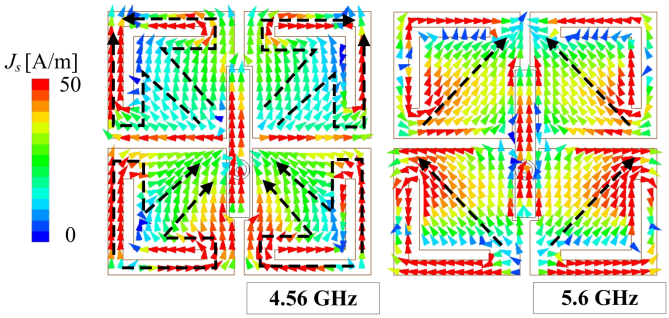


Fig. 3. Simulated current distributions at different frequencies of the dual-band antenna.

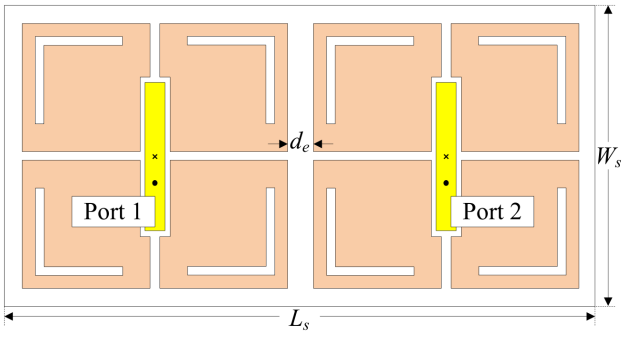


Fig. 4. Geometry of the coupled MIMO antenna. $L_s = 60$ mm, $W_s = 30$ mm, $d_e = 4$ mm.

II. Dual-Band Antenna

A. Antenna Design

Fig. 1 shows the geometrical configuration of the proposed single-layer dual-band antenna, which is developed from the single-layer single-band design in [22]. It should be noted that our previous work [22] focused exclusively on a single-band antenna, whereas the present study extends that concept to dual-band operation and a MIMO configuration. The antenna is designed on a Taconic RF-35 substrate with dielectric constant of 3.5 and loss tangent of 0.0018. The radiating element comprises four square patches arranged around a centrally located rectangular feeding patch. The central rectangular patch is excited by a coaxial probe and capacitively couples electromagnetic energy to the four surrounding square patches through the gaps between them. To realize dual-band operation, four slots are embedded into the square patches. The antenna is modeled and analyzed using the full-wave electromagnetic solver Ansys High-Frequency Structure Simulator (HFSS). The optimal dimensions of the single-layer dual-band antenna are as follows: $W_s = 30$, $l_p = 14.6$, $w_p = 2.6$, $d = 2.6$, $g = 0.3$, $s = 1.0$, $W_o = 12.5$, $l_c = 8.0$, $w_c = 1.0$, $t = 1.5$ (unit: mm).

B. Antenna Operation

Fig. 2 illustrates the simulated reflection coefficient ($|S_{11}|$) and realized gain of the proposed dual-band antenna. As observed, two well-defined resonant modes are excited at approximately 4.6 and 5.6 GHz. The antenna maintains a stable realized gain of better than 6.0 dBi across both operating bands.

To clarify the dual-band mechanism, Fig. 3 presents the simulated surface current distributions of the dual-band antenna at 4.6 and 5.6 GHz. As observed, the introduction of the slots disturbs the current path and breaks the original symmetry of the patch. As a result, the induced currents in the dual-band antenna tend to flow along diagonal directions. At 4.6 GHz, the current is mainly concentrated along the embedded slot, indicating that the slot-loaded path is primarily responsible for the lower-band resonance. At 5.6 GHz, however, the current flows along the other diagonal direction of the patch, corresponding to the upper-band resonance.

III. Coupled MIMO Antenna

The MIMO antenna is developed from the dual-band element presented in the previous section, as shown in Fig. 4. In this configuration, two identical radiating elements are placed side by side with an edge-to-edge separation of $d_e = 4$ mm.

The corresponding simulated reflection and transmission coefficients, ($|S_{11}|$) and ($|S_{21}|$), are presented in Fig. 5.

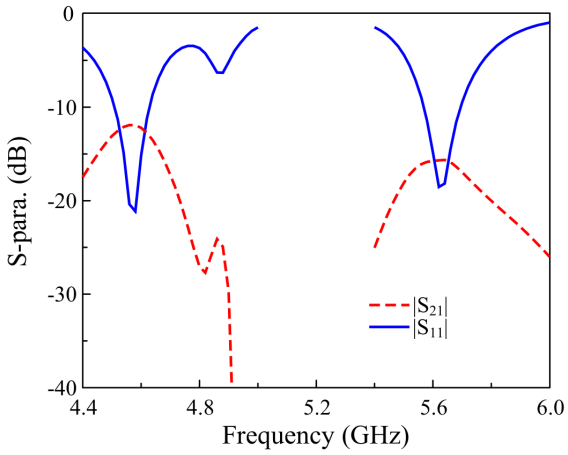


Fig. 5. Simulated S-parameter of the coupled MIMO antenna.

The antenna maintains dual-band operation, with a lower-band impedance bandwidth of 4.51–4.63 GHz and an upper-band bandwidth of 5.57–5.69 GHz. However, stronger mutual coupling is observed in the lower band, where the isolation is approximately 12 dB. In contrast, the upper band exhibits improved isolation of about 16 dB over the operating bandwidth. This improvement can be explained by the smaller effective resonator size at the upper band, which results in a larger relative separation between the active radiating patches and consequently reduces inter-element coupling.

IV. Decoupled MIMO Antenna

A. Design 1

To reduce mutual coupling, a decoupling structure is introduced. Fig. 6 shows the geometry of the decoupled MIMO antenna, referred to as Design 1. Four shorting vias are placed at the corners of the adjacent patches. These vias provide additional inductive loading and, together with the capacitance formed by the adjacent patches and narrow gaps, create compact transmission zero around the operating bands. As a result, the dominant coupling path between the two ports is effectively suppressed, thereby improving the inter-element isolation.

For validation, Fig. 7 presents the simulated S-parameters of the decoupled MIMO antenna. As observed, the isolation in the lower band is significantly improved to better than 27 dB across the operating bandwidth. In contrast, the isolation in the upper band remains almost unchanged. This is because the shorting vias are located at the corners of the adjacent patches, where the dominant inter-element coupling in the lower band is mainly concentrated.

When the vias are shifted along the x-direction toward the blue-color region, the lower-band isolation deteriorates, as shown in Fig. 8. However, as the vias approach the region where strong upper-band coupling occurs, the isolation in the higher band can be enhanced. These results confirm that the position of the shorting vias plays an important role in controlling the decoupling performance at each operating band.

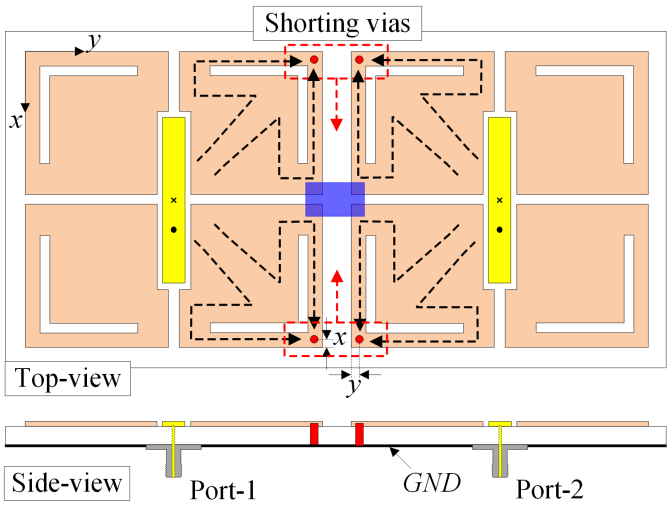


Fig. 6. Geometry of the decoupled MIMO antenna, Design 1. $x = 0.5$ mm, $y = 0.5$ mm.

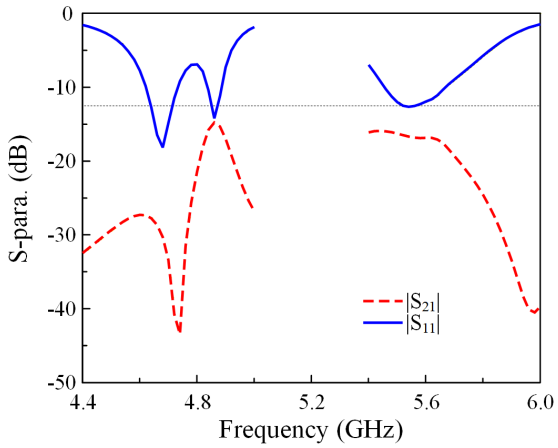


Fig. 7. Simulated S-parameter of the decoupled MIMO antenna, Design 1.

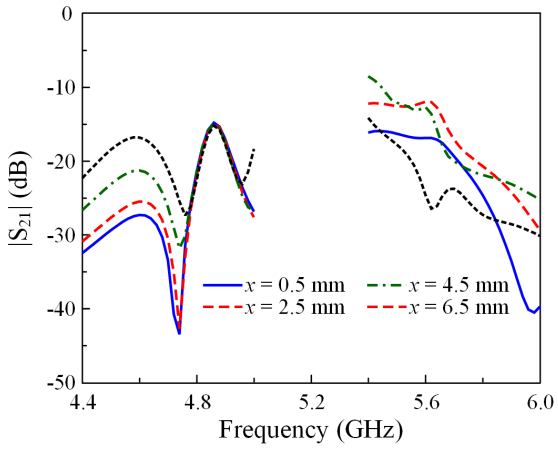


Fig. 8. Simulated S-parameter of the decoupled MIMO antenna, Design 1, for different positions of shorting vias, x.

B. Design 2

Based on the above analysis, additional shorting vias, indicated in blue, are introduced at the regions where strong upper-band coupling is concentrated. Fig. 9 shows the geometry

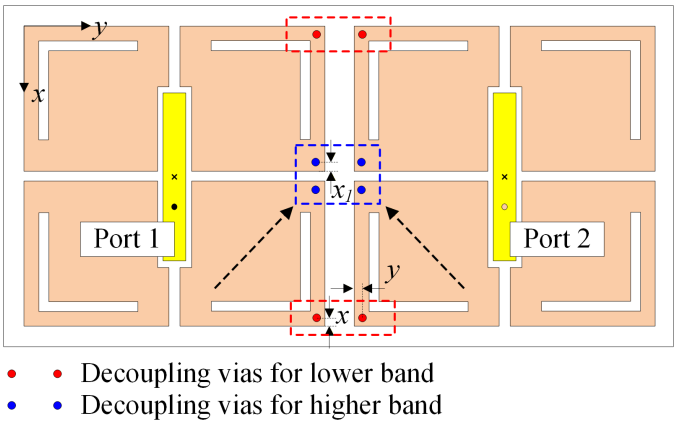


Fig. 9. Geometry of the decoupled MIMO antenna, Design 2.

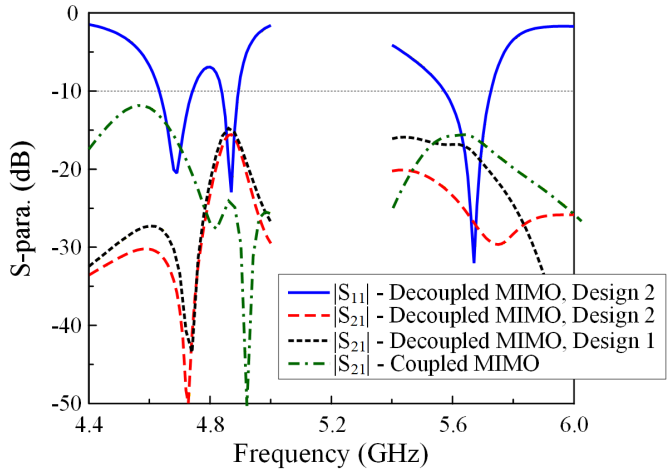
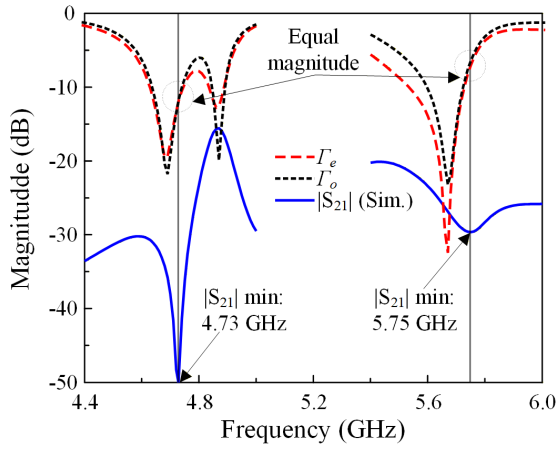
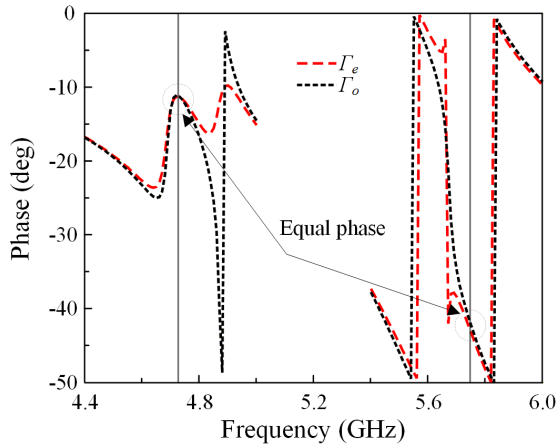


Fig. 10. Simulated S-parameter of the decoupled MIMO antenna, Design 2.



(a)



(b)

Fig. 11. Even- and odd-mode eigen-reflections of the decoupled MIMO antenna, Design 2. (a) Magnitude, and (b) phase.

of the final proposed MIMO antenna. In this configuration, the first set of shorting vias mainly suppresses the coupling associated with the lower-band resonant mode, while the additional vias are used to control the coupling path of the upper-band mode. Since the field distributions and current paths are different at the two operating bands, placing the vias at the corresponding high-coupling regions enables effective isolation improvement without requiring extra decoupling space between the elements.

The simulated S-parameters of the final design are shown in Fig. 10. As observed, high isolation is achieved in both operating bands. The lower band covers 4.63–4.74 GHz, with isolation better than 30 dB across the entire bandwidth. Meanwhile, the upper band exhibits good impedance matching from 5.57 to 5.73 GHz, while maintaining isolation higher than 24 dB. Compared with the previous design, the additional shorting vias significantly improve the upper-band isolation while preserving the high isolation in the lower band. This confirms that the proposed via-loading strategy can independently control the dominant coupling paths at different resonant modes, leading to compact and effective dual-band decoupling performance.

C. Decoupling Mechanism

For symmetric two-port MIMO antenna, the S-matrix is defined as follows:

$$S = \begin{bmatrix} S_{11} & S_{21} \\ S_{21} & S_{11} \end{bmatrix} \tag{1}$$

The eigenvalues of this matrix correspond to the even and odd modes:

$$\Gamma_e = S_{11} + S_{21} \quad \text{and} \quad \Gamma_o = S_{11} - S_{21} \tag{2}$$

Accordingly,

$$S_{21} = \frac{\Gamma_e - \Gamma_o}{2} \tag{3}$$

For the case without vias, the strong electromagnetic interaction between the two antennas makes the even- and odd-mode boundary conditions substantially different, resulting in $\Gamma_e \neq \Gamma_o$. Accordingly, strong mutual coupling between the MIMO elements, and then poor isolation.

The isolation can be significantly changed with the presence of shorting vias, which act as reactive loading elements. Together with the inter-patch capacitance, they modify the

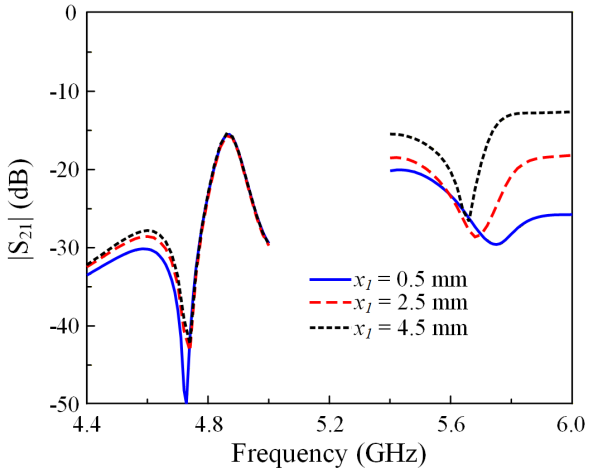


Fig. 12. Simulated $|S_{21}|$ of the decoupled MIMO antenna, Design 2, for different positions of the second via set.

magnitude and phase of the mutual-coupling path and bring the complex even- and odd-mode reflection coefficients toward equality. It can be seen obviously in Fig. 11 that at two minimum $|S_{21}|$ point at 4.73 and 5.75 GHz corresponding to two operating bands, the magnitude and phase of Γ_e and Γ_o are quite similar. Consequently, S_{21} approaches zero, producing a transmission zero and substantially enhancing port isolation.

The position of the shorting vias is critical to determining the isolation of each band. As shown in Fig. 8, which shows the $|S_{21}|$ of the decoupled MIMO with one set of shorting vias, Design 1. The results demonstrate that the via position is important, and a shorting via is effective only if it is positioned in a strong electric/magnetic field region. When moving it far from the strong current of lower band, the isolation in this band degrades. In the meantime, the shorting via is getting closer to the strong field of higher band. Consequently, the isolation in the higher band can be improved, especially at 6.5 mm. For the final decoupled MIMO, Design 2, Fig. 12 shows the effect of second via set on the isolation feature. Obviously, it mostly affect isolation characteristic in the higher band. Regarding the matching performance, the second via set has small effect at both bands and thus, the results are not shown for brevity.

V. Measurement Results

For verification, an antenna prototype is fabricated and measured. Fig. 13 shows the photographs of the fabricated prototype and its measurement setup with ROHDE & Schwarz ZNB20 vector Network Analyzer. Overall, the simulation and measurement are well-matched. A tolerance from fabrication and measurement setup are minor. The simulated and measured performances in terms of S-parameter and peak realized gain are depicted in Figs. 14 and 15. As observed, the antenna shows good performance at both bands.

The measured operating bandwidths are 2.8% (4.62 - 4.75 GHz) and 3.9% (5.50 - 5.72 GHz) at lower and upper bands, respectively. Across the lower band operation, the isolation is from 29 to 43 dB. Meanwhile, that for higher band is from 25 to 33 dB. Due to the symmetrical configuration of the MIMO

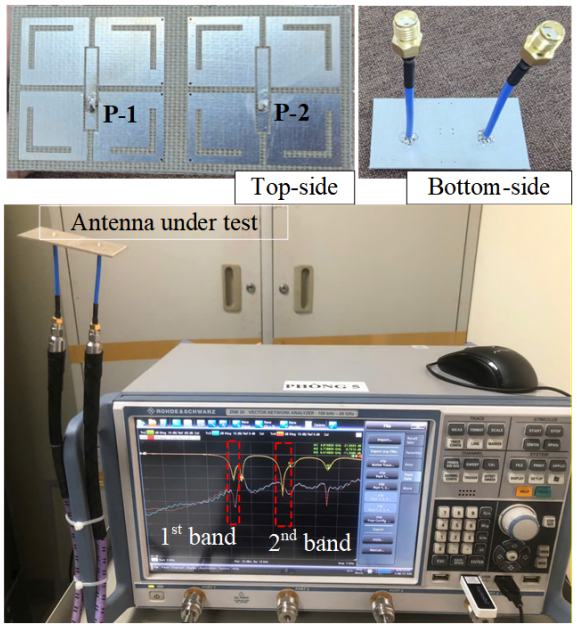


Fig. 13. Fabricated prototype and measurement setup of the proposed MIMO antenna

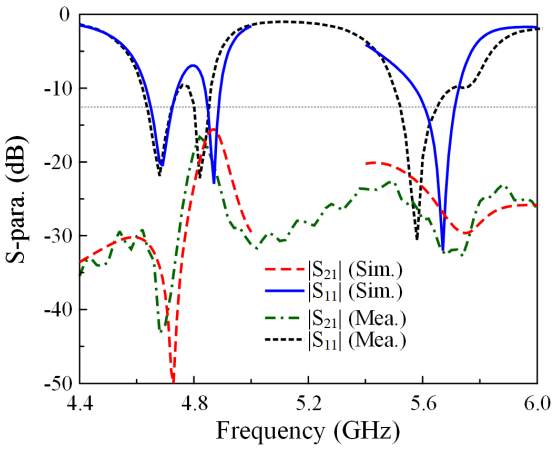


Fig. 14. Simulated and measured S-parameter of the proposed MIMO antenna.

antenna, the measured peak realized gains for both Port 1 and Port 2 are nearly identical, ranging from 4.8 to 5.4 dBi for the 4.6 GHz band and 5.2 to 6.8 dBi for the 5.6 GHz band. The good agreement between the simulated and measured gains suggests that the measured radiation efficiency is expected to be close to the simulated value of approximately 90%.

The simulated and measured radiation patterns at 4.64 and 5.68 GHz are shown in Fig. 16. Owing to the symmetrical antenna configuration, only the results for Port 1 excitation are presented for brevity. The antenna exhibits stable and well-defined radiation patterns 5-GHz Wi-Fi.

The measured operating bandwidths are 130 and 220 MHz for the lower and upper bands, respectively. The lower-band bandwidth specifically covers the 4.62–4.75 GHz portion of the Sub-6 GHz n79 5G NR band (which spans from 4.4 to 5.0 GHz), supporting channel bandwidths up to 100 MHz. For

TABLE I
PERFORMANCE COMPARISON AMONG SINGLE-LAYER DUAL-BAND MIMO ANTENNAS

Ref.	Dimensions (λ)	Decoupling structure	Edge spacing (λ)	Isolation (dB)	1st band		2nd band	
					BW (%)	Peak gain (dBi)	BW (%)	Peak gain (dBi)
[16]	$0.42 \times 0.21 \times 0.05$	Metalized walls	0.03	≥ 18	1.6	2.7	0.7	2.8
[17]	Not Given	C-shaped patch	0.06	≥ 20	2.5	Not Given	2.2	Not Given
[18]	$1.14 \times 0.68 \times 0.02$	Loop resonator	0.06	≥ 25	2.9	5.9	2.4	5.9
[19]	$0.60 \times 0.40 \times 0.03$	Shorting vias	0.03	≥ 15	≤ 1.0	5.0	≤ 1.0	6.0
[20]	$0.62 \times 0.40 \times 0.03$	90° rotation	0.06	≥ 15	11.4	3.6	4.5	2.4
[21]	$1.40 \times 0.70 \times 0.03$	90° rotation	0.41	≥ 20	25.7	8.9	20.4	8.7
Prop.	$\mathbf{0.94 \times 0.47 \times 0.02}$	**Shorting vias**	**0.06**	$\geq$ **25**	**2.8**	**5.4**	**3.9**	**6.8**

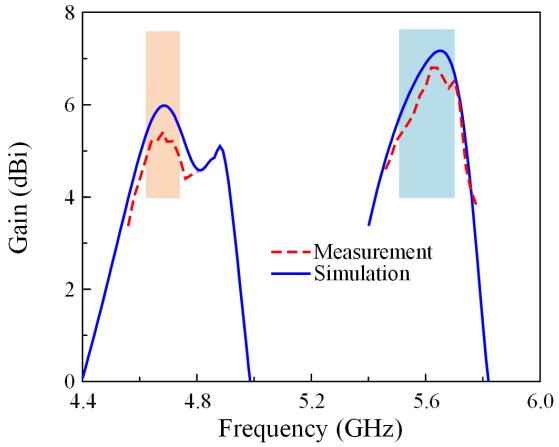


Fig. 15. Simulated and measured realized gain of the proposed MIMO antenna.

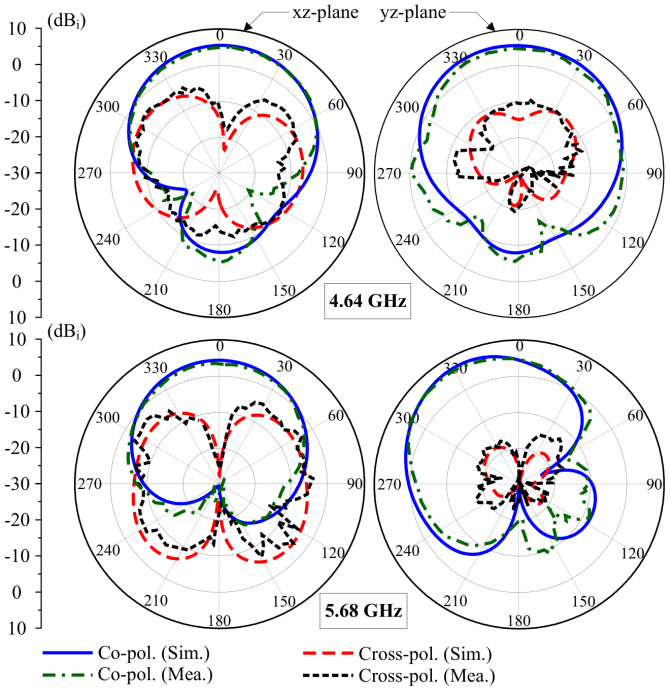


Fig. 16. Simulated and measured radiation patterns of the proposed MIMO antenna.

the upper band, the 220 MHz bandwidth (5.50–5.72 GHz) can accommodate common 5-GHz Wi-Fi channel bandwidths up to 160 MHz. Therefore, the proposed antenna is highly suitable for compact dual-band MIMO operation within these specific 5G NR and Wi-Fi frequency ranges, while maintaining high isolation and stable realized gain across the measured bands.

VI. MIMO DIVERSITY PERFORMANCE

To evaluate the MIMO diversity performance of the proposed antenna, four important parameters including Envelope Correlation Coefficient (ECC), Mean Effective Gain (MEG), Total Active Reflection Coefficient (TARC), and Channel Capacity Loss (CCL) are discussed. According to [23], these parameters are calculated based on simulated and measured S-parameters. Fig. 17 shows the simulated and measured ECC, MEG, TARC, and CCL of the proposed design.

The simulated and measured diversity parameters show good agreement and confirm satisfactory MIMO performance of the proposed antenna. As shown in Fig. 17, the ECC remains close to zero in both operating bands, indicating very low correlation between the two antenna ports. The MEG values are approximately -3 dB within the operating bands, with only small differences between simulation and measurement, indicating balanced power reception. Moreover, the TARC remains below -10 dB, demonstrating good active impedance matching under simultaneous port excitation, while the CCL is maintained below the commonly accepted limit of 0.4 bits/s/Hz. Overall, the low ECC and CCL together with satisfactory MEG and TARC values demonstrate that the proposed antenna meets the practical diversity requirements for MIMO operation.

VII. PERFORMANCE COMPARISON

Table I compares the proposed antenna with previously reported dual-band MIMO antennas. Compared with [16], [19], and [20], the proposed antenna provides higher gain 5-GHz Wi-Fi while maintaining much better isolation. Although [21] achieves wider bandwidth and higher gain, it requires a significantly larger footprint. In contrast, the proposed design has a more compact profile while still achieving peak gains of 5.4 and 6.8 dBi at the first and second bands, respectively. Moreover, the isolation is better than 25 dB, which is comparable to or higher than most reported designs. Therefore, the proposed antenna offers a good trade-off among compact

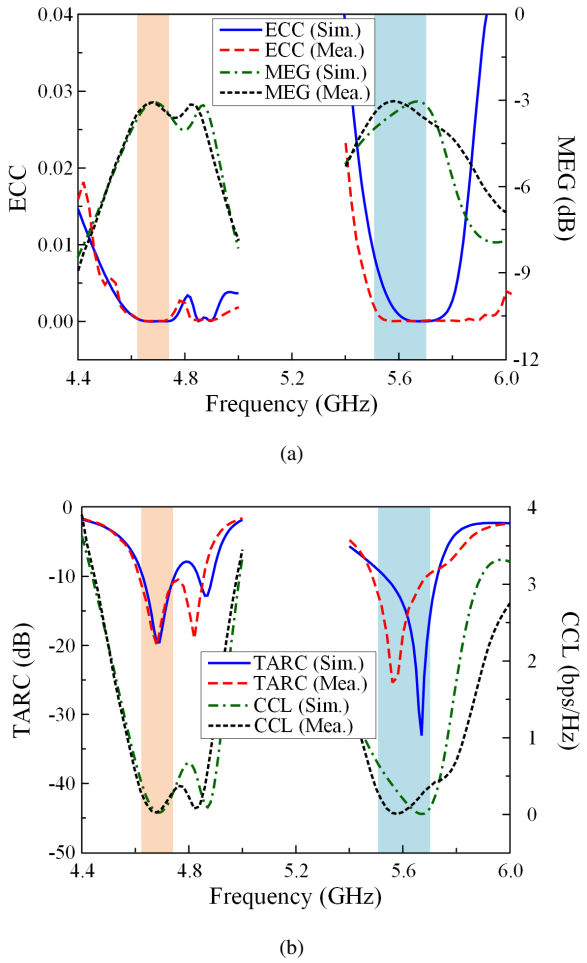


Fig. 17. Simulated and measured (a) ECC and MEG, (b) TARC and CCL of the proposed antenna.

size, high isolation, and stable gain for dual-band MIMO applications.

VIII. Conclusion

A compact single-layer dual-band two-port MIMO antenna has been proposed and investigated. Dual-band operation is achieved using four slotted square patches capacitively coupled to a centrally located probe-fed patch. To enhance port isolation, shorting vias are incorporated as compact decoupling elements, providing the transmission zero behavior that effectively suppresses mutual coupling in both operating bands. The fabricated prototype occupies only $0.94\lambda \times 0.47\lambda \times 0.02\lambda$ at 4.6 GHz. The measured results show impedance bandwidths of 4.62 - 4.75 GHz and 5.50 - 5.72 GHz, corresponding to 2.8% and 3.9% for both bands. Across these bands, the antenna achieves isolation greater than 25 dB, alongside stable realized gains of 4.8–5.4 dBi for the 4.6 GHz band and 5.2–6.8 dBi for the 5.6 GHz band at both individual ports. These results demonstrate that the proposed antenna is a promising candidate for compact dual-band MIMO systems, specifically covering the 4.62-4.75 GHz range of the Sub-6 GHz 5G NR n79 band (4.4–5.0 GHz) and the 5.50–5.72 GHz range for 5-GHz Wi-Fi applications. Future work focuses on extending the current design for multi-port MIMO systems.

Acknowledgments

This work was supported by the Vietnam National Foundation for Science and Technology Development (NAFOSTED) under Grant number 102.04-2023.28.

References

[1] 3GPP, "NR; User Equipment (UE) radio transmission and reception; Part 1: Range 1 Standalone," Technical Specification (TS) 38.101-1.

[2] IEEE, "IEEE Standard for Information technology–Telecommunications and information exchange between systems–Local and metropolitan area networks–Specific requirements–Part 11: Wireless LAN MAC and PHY Specifications–Amendment 4: Enhancements for Very High Throughput for Operation in Bands below 6 GHz," Tech. Rep. IEEE Std 802.11ac-2013, 2013.

[3] H.-L. Peng, R. Tao, W.-Y. Yin, and J.-F. Mao, "A novel compact dual-band antenna array with high isolations realized using the neutralization technique," *IEEE Transactions on Antennas and Propagation*, vol. 61, no. 4, pp. 1956–1962, Apr. 2013. doi: 10.1109/tap.2012.2234714

[4] J.-H. Xun, L.-F. Shi, W.-R. Liu, G.-X. Liu, and S. Chen, "Compact dual-band decoupling structure for improving mutual coupling of closely placed pifas," *IEEE Antennas and Wireless Propagation Letters*, vol. 16, pp. 1985–1989, 2017. doi: 10.1109/lawp.2017.2691716

[5] X. Shen, F. Liu, L. Zhao, G.-L. Huang, X. Shi, Q. Huang, and A. Chen, "Decoupling of two strongly coupled dual-band antennas with reactively loaded dummy element array," *IEEE Access*, vol. 7, pp. 154 672–154 682, 2019. doi: 10.1109/access.2019.2948897

[6] J. Sui and K.-L. Wu, "A general t-stub circuit for decoupling of two dual-band antennas," *IEEE Transactions on Microwave Theory and Techniques*, vol. 65, no. 6, pp. 2111–2121, 2017. doi: 10.1109/tmtt.2017.2647951

[7] K.-D. Xu, H. Luyen, and N. Behdad, "A decoupling and matching network design for single- and dual-band two-element antenna arrays," *IEEE Transactions on Microwave Theory and Techniques*, vol. 68, no. 9, pp. 3986–3999, 2020. doi: 10.1109/tmtt.2020.2989120

[8] L. Zhao and K.-L. Wu, "A dual-band coupled resonator decoupling network for two coupled antennas," *IEEE Transactions on Antennas and Propagation*, vol. 63, no. 7, pp. 2843–2850, 2015. doi: 10.1109/tap.2015.2421973

[9] C. Munusami and R. Venkatesan, "A compact boat shaped dual-band mimo antenna with enhanced isolation for 5g/wlan application," *IEEE Access*, vol. 12, pp. 11 631–11 641, 2024. doi: 10.1109/access.2024.3356078

[10] J. Liu, H. Liu, X. Dou, Y. Tang, C. Zhang, L. Wang, R. Tang, and Y. Yin, "A low profile, dual-band, dual-polarized patch antenna with antenna-filter functions and its application in mimo systems," *IEEE Access*, vol. 9, pp. 101 164–101 171, 2021. doi: 10.1109/access.2021.3096969

[11] Z. Niu, H. Zhang, Q. Chen, and T. Zhong, "Isolation enhancement in closely coupled dual-band mimo patch antennas," *IEEE Antennas and Wireless Propagation Letters*, vol. 18, no. 8, pp. 1686–1690, Aug. 2019. doi: 10.1109/lawp.2019.2928230

[12] A. E. Farahat and K. F. A. Hussein, "Dual-band (28/38 ghz) wideband mimo antenna for 5g mobile applications," *IEEE Access*, vol. 10, pp. 32 213–32 223, 2022. doi: 10.1109/access.2022.3160724

[13] Z. Zahid, G. Sun, H. Li, H. Chen, K.-Y. Jung, H. Wang, and L. Qu, "Dual-band single-patch mimo antenna with capacitor-loaded shorting posts (clsps) as modal tuners," *IEEE Antennas and Wireless Propagation Letters*, vol. 24, no. 6, pp. 1482–1486, 2025. doi: 10.1109/lawp.2025.3540870

[14] F. Liu, J. Guo, L. Zhao, G.-L. Huang, Y. Li, and Y. Yin, "Dual-band metasurface-based decoupling method for two closely packed dual-band antennas," *IEEE Transactions on Antennas and Propagation*, vol. 68, no. 1, pp. 552–557, Jan. 2020. doi: 10.1109/tap.2019.2940316

[15] W. Zhang, Y. Li, K. Wei, and Z. Zhang, "A dual-band mimo antenna system for 2.4/5 ghz wlan applications," *IEEE Transactions on Antennas and Propagation*, vol. 71, no. 7, pp. 5749–5758, 2023. doi: 10.1109/tap.2023.3277208

[16] A. Boukarkar, X. Q. Lin, Y. Jiang, L. Y. Nie, P. Mei, and Y. Q. Yu, "A miniaturized extremely close-spaced four-element dual-band mimo antenna system with polarization and pattern diversity," *IEEE Antennas and Wireless Propagation Letters*, vol. 17, no. 1, pp. 134–137, Jan. 2018. doi: 10.1109/lawp.2017.2777839

[17] N. Ojaroudi Parchin, Y. I. A. Al-Yasir, H. J. Basherlou, and R. A. Abd-Alhameed, "A closely spaced dual-band mimo patch antenna with reduced mutual coupling for 4g/5g applications," *Progress In Electromagnetics Research C*, vol. 101, pp. 71–80, 2020. doi: 10.2528/pierc20013001

[18] B. L. Dhevi, K. S. Vishvaksenan, and K. Rajakani, "Isolation enhancement in dual-band microstrip antenna array using asymmetric loop resonator," *IEEE Antennas and Wireless Propagation Letters*, vol. 17, no. 2, pp. 238–241, Feb. 2018. doi: 10.1109/lawp.2017.2781907

[19] J. C. Dash and D. Sarkar, "A four-port csrr-loaded dual-band mimo antenna with suppressed higher order modes," *IEEE Access*, vol. 10, pp. 30 770–30 778, 2022. doi: 10.1109/access.2022.3160831

[20] X.-H. Ding, Z. Tan, and S. N. Burokur, "A compact single layer dual band microstrip patch antenna for 5g terminal applications," *Scientific Reports*, vol. 15, no. 1, Mar. 2025. doi: 10.1038/s41598-025-93592-3

[21] W. A. Awan, A. Abbas, D. Choi, N. Hussain, H. Lee, D. Sim, and N. Kim, "Compact and directional dual band antenna with low mutual coupling mimo configuration for mm-wave communication," *Results in Engineering*, vol. 26, p. 105457, 2025. doi: 10.1016/j.rineng.2025.105457

[22] T. Dao-Duc, N. Truong-Quang, T. Le-Tuan, and H. Tran-Huy, "High front-to-back ratio metasurface antenna with single-layer and compact size for wlan applications," *PLOS One*, vol. 20, no. 5, p. e0321603, May 2025. doi: 10.1371/journal.pone.0321603

[23] A. Chakraborty, R. S. Saxena, I. Singh, J. Kaur, R. Kaur, R. Kalia, and D. D. Bhavani, "Defected ground structure (dgs) based mimo antenna array with decent isolation characteristics for satellite communications in unified s-band (usb)," *Radio Science*, vol. 60, no. 11, Nov. 2025. doi: 10.1029/2025rs008379



Yem Vu-Van received his bachelor's and master's degrees from Hanoi University of Science and Technology, Vietnam. He received his Ph.D. in Electronics and Telecommunication Engineering from Télécom ParisTech in 2005. He is currently a full professor in the School of Electrical and Electronic Engineering at Hanoi University of Science and Technology. His main research interests include multi-antenna wireless communication systems, antennas, and ultra-high-frequency techniques.



Thao Hoang-Thi-Phuong received her Dipl. of Engineer (2004), Master of Science (2007), and PhD degree (2019) in Electronics and Telecommunications from Hanoi University of Science and Technology, Vietnam. Currently, she is a lecturer at Electronics and Telecommunications Faculty, Electric Power University, Vietnam. Her research interests include designing antennas, localization systems, and wireless communication systems.



Quyen Nguyen-Xuan received his Diploma of Engineering, master's, and Ph.D. degrees in electronics and telecommunications, in 2006, 2008, and 2013, respectively. He was an exchange Ph.D. Student with the Institute for Smart System Technologies, Alpen-Adria Klagenfurt University, Austria, from 2011 to 2012. From 2014 to 2015, he was a Postdoctoral Researcher with the Department of Computer Architecture, Polytechnic University of Catalonia (UPC BarcelonaTech), Spain. He was also an Academic Visitor with the Department of Electronic and Computer Engineering, University of Limerick, Ireland, in 2015, the School of Electronics, Electrical Engineering and Computer Science, Queen's University Belfast, U.K., in 2016, and the Department of Computer and Network Engineering, The University of Electro-Communications, Tokyo, Japan, in 2017. Since 2017, he has been a Senior Lecturer and an Associate Professor with the School of Electrical and Electronic Engineering (SEEE), Hanoi University of Science and Technology (HUST), Vietnam. His research interests include microwave design and implementation, chaos-based digital communications, physical layer security, and wireless communications.



Cuong Do-Manh serves as a dedicated academic and researcher within the Faculty of Electrical and Electronic Engineering at the Phenikaa School of Engineering, Phenikaa University, Hanoi, Vietnam. He is actively engaged in the rigorous study of microwave systems, antenna and propagation, and the practical design of high-performance antennas. His ongoing research initiatives explore modern solutions for efficient wireless transmission and electromagnetic wave behavior, playing a vital role in the scientific output and technological advancements of his institution.